

Bose glass transition in columnar-defected untwinned $\text{YBa}_2\text{Cu}_3\text{O}_{7-\delta}$

Robert J. Olsson, Wai-Kwong Kwok, Lisa M. Paulius,* Andra M. Petrean,* David J. Hofman,[†] and George W. Crabtree
Materials Science Division, Argonne National Laboratory, Argonne, Illinois 60439

(Received 31 May 2001; revised manuscript received 15 August 2001; published 1 March 2002)

We demonstrate the Bose glass scaling behavior in a single crystal of $\text{YBa}_2\text{Cu}_3\text{O}_{7-\delta}$ (YBCO) free from twin boundary pinning. We determine the scaling exponents from voltage-current measurements near the transition temperature and infer a lock-in transition from measurements of the angular dependence of the resistivity. In addition we demonstrate that the kink in the Bose glass irreversibility line in irradiated untwinned YBCO occurs systematically at the dose matching field.

DOI: 10.1103/PhysRevB.65.104520

PACS number(s): 74.60.Ge, 74.25.Dw, 74.25.Fy

The effect of carefully controlled irradiation-induced disorder on the vortex phase diagram of the high-temperature superconductor $\text{YBa}_2\text{Cu}_3\text{O}_{7-\delta}$ has been studied extensively in recent years.¹⁻⁴ In clean crystals of $\text{YBa}_2\text{Cu}_3\text{O}_{7-\delta}$, thermodynamic measurements⁵⁻⁸ have established a first-order vortex lattice to liquid transition. With the introduction of increasing disorder, first-order transitions are generally expected to transform into continuous transitions.⁹ In $\text{YBa}_2\text{Cu}_3\text{O}_{7-\delta}$ (YBCO), a variety of disordered vortex solid states have been proposed, depending on the type and dimensionality of the disorder. In the presence of weak random point disorder, a vortex glass phase¹⁰ or a polymerlike glass phase¹¹ has been predicted, whereas in the presence of correlated disorder, a Bose glass phase¹² is expected. Both types of defects can transform the first-order vortex melting transition into a second-order transition, giving rise to a critical regime dominated by diverging correlation lengths. However, there are marked differences. The vortex glass phase is characterized by isotropic pinning due to point disorder, whereas the Bose glass phase is characterized by anisotropic pinning due to correlated defects, represented, for example, by one-dimensional columnar tracks induced by heavy-ion irradiation or by two-dimensional planar twin boundaries. Several experiments claiming to demonstrate the existence of these two phases have been reported. However, earlier experiments contained preexisting defects in the sample leading to ambiguity as to the nature of the glassy phase. In many cases, what was reported as a vortex glass phase^{13,14} in YBCO thin films and crystals may in fact be more related to a Bose glass phase due to the existence of twin boundaries in the samples.¹⁵⁻¹⁷ In addition to acting as correlated defects, twin boundaries can also introduce added complications in transport measurements due to such phenomena as guided motion of the vortices parallel to a twin plane.¹⁸⁻²⁰ Many of the previous studies on YBCO crystals with columnar defects induced by heavy-ion irradiation were performed on twinned crystals, confounding the separation of vortex localization by columnar defects from twin boundary pinning. Although in some of the earlier studies, the crystals contained only widely spaced twin planes about $1\ \mu\text{m}$ apart,^{15,16} other measurements have shown that even two twin boundaries can have a dramatic effect on pinning, especially at temperatures near T_c .²¹ It has also been noted that approximately the same critical scaling behavior has been observed in thick films of YBCO both before and after heavy-ion ir-

radiation due to the presence of twin boundaries and edge dislocations.²² Recent measurements on twin-free crystals with the field tipped off the columnar defect direction show glassy transitions apparently outside the classical Bose glass description.²³ Indeed, the demise of a transverse Meissner effect associated with the Bose glass was found to lie several tens of Kelvin below the disappearance of the linear resistivity, suggesting an intermediate vortex regime where vortices are pinned against lateral motion arising from transport currents but are allowed to change their orientation in response to the applied field direction. Thus, to our best knowledge, a definitive investigation of the Bose glass transition in YBCO is still lacking.

In this paper we show unambiguous evidence for a Bose glass transition in a completely untwinned single crystal of YBCO, irradiated with heavy ions to induce straight columnar defects in the sample. Unlike previous studies on weakly twinned crystals,^{15,16} our unirradiated and untwinned crystals show a clear first-order vortex melting transition, demonstrating their high quality and nearly defect-free nature. We determine the static and dynamic critical exponents ν and z , respectively, associated with the Bose glass scaling theory from voltage-current scaling behavior and compare them with those obtained from the angular dependence of the resistivity. In addition, we find a sharp kink in the Bose glass irreversibility line at the dose matching field,²⁴ where the density of columnar defects equals the density of vortices. The position of the kink scales directly with the dose matching field, indicating a fundamental change in the vortex pinning behavior when vortices outnumber columnar defects.

Single crystals of YBCO were prepared using the flux-growth method. The crystals were detwinned by applying uniaxial pressure at $420\ \text{°C}$ in flowing oxygen and then polished down to less than $30\ \mu\text{m}$ along the c axis to ensure that the heavy ions traverse the entire cross section of the sample, as described by TRIM calculations.^{25,26} No vestiges of twins were observed by polarized light microscopy after detwinning. Two crystals were cleaved from a larger single piece ($780 \times 740 \times 19\ \mu\text{m}^3$). One crystal was irradiated with $1.4\text{-GeV}\ ^{208}\text{Pb}^{56,4+}$ ions along the crystallographic c axis to a dose matching field of $B_\phi = 1\ \text{T}$ and the second cleaved piece was kept as a reference. Cleaving the crystals from a larger piece for this experiment ensures that the starting underlying quality of the crystals prior to irradiation is equivalent.

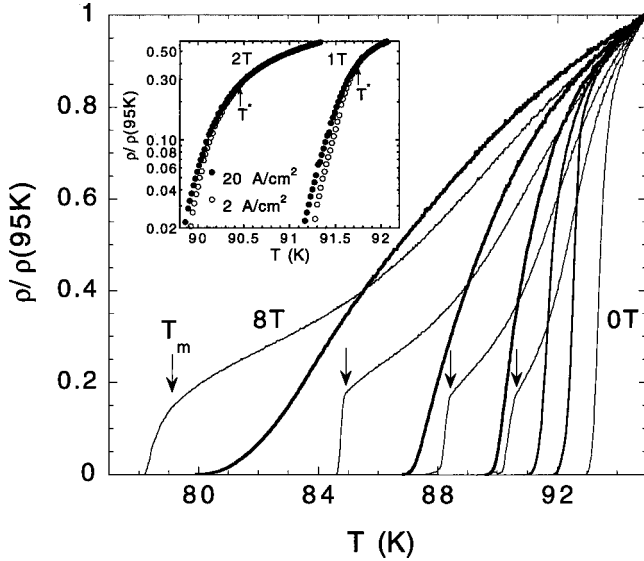


FIG. 1. Normalized resistivity versus temperature for the unirradiated reference crystal (thin lines) and the $B_\phi = 1$ T Pb-ion irradiated crystal (thick lines) for $H = 0, 1, 2, 4,$ and 8 T. The arrows mark the first-order melting temperature T_m for the unirradiated crystal. Inset: Semilog plot of the temperature-dependent resistivity of the irradiated crystal at $H = 1$ and 2 T measured with two different transport currents. Arrows indicate the onset of nonohmic behavior at T^* .

Transport measurements were carried out using the standard four-probe technique. Gold contacts were first evaporated onto the surface of the crystal and sintered at 420°C . Gold wires were subsequently attached to the contacts with silver epoxy, resulting in contact resistances of about $1\ \Omega$. Ac resistivity measurements were performed with transport current densities typically in the range of 2 to $20\ \text{A/cm}^2$ at $23\ \text{Hz}$. Dc resistivity and I - V measurements were carried out with a nanovoltmeter using current reversal to minimize thermal effects. The crystal was placed in the center of a 1.5 -T superconducting split coil magnet that resides in the bore of an 8 -T superconducting solenoid magnet. The magnetic field could be rotated with respect to the sample by energizing the magnets independently. For the irradiated crystals, θ is defined as the angle between the applied magnetic field and the columnar defect direction. The measuring current was applied in the ab plane and perpendicular to the applied magnetic field and columnar defect directions.

Figure 1 shows the temperature dependence of the resistivity for the unirradiated reference crystal (thin lines) and the irradiated crystal (thick lines). The zero-field superconducting transition of the crystal before irradiation is $T_{co} = 93.83\ \text{K}$ with width $\Delta T_{co} \sim 300\ \text{mK}$. After irradiation, $T_{co} = 92.57\ \text{K}$, with a slight broadening of the transition width to $\Delta T_{co} \sim 500\ \text{mK}$, and the normal-state resistivity increased by approximately 6% . The high quality of the unirradiated crystal is underlined by the sharp kink in the resistivity associated with the first-order vortex lattice freezing transition.²⁷ The onset of the sharp kink at T_m also separates ohmic resistive behavior above from nonohmic resistive behavior below this temperature. After irradiation with a dose

matching field of $B_\phi = 1\ \text{T}$, the kink representing the first-order vortex melting transition is completely suppressed and replaced with a smooth decrease in the resistivity at all measured fields, reaching zero resistivity at a much higher temperature than the first-order vortex melting temperature.

Although the kink associated with first-order melting is absent after irradiation, the initial overlap and subsequent splitting of two resistivity curves measured at 2 and $20\ \text{A/cm}^2$ indicates that nonohmic behavior persists below a characteristic temperature T^* as shown by the arrows in the inset to Fig. 1. The disappearance of the kink suggests that the transition is no longer first order, and the appearance of nonohmic behavior at more than 30% of the normal-state resistance $\rho(95\ \text{K})$ demonstrates that vortex motion in the liquid state is dramatically affected by the columnar defects. It is within this measurable nonlinear fluctuation regime that the Bose glass critical scaling theory applies. The inset to Fig. 1 also shows that both T^* and the normalized resistivity ρ_{irr}/ρ_n , where nonohmic behavior occurs, shift down in magnitude with increasing field.

In the presence of correlated defects, the Bose glass theory predicts a continuous transition that is described by transverse and longitudinal correlation lengths given by $l_\perp \sim 1/|T_{\text{Bg}} - T|^\nu$ and $l_\parallel \sim l_\perp^2$, respectively, where T_{Bg} is the Bose glass transition temperature, and ν is a critical scaling exponent.¹² The relaxation time of a fluctuation is expected to diverge with a dynamic scaling exponent z , given by $\tau \sim l_\perp^z$. From the anisotropic Ginzburg-Landau free energy, the current density $J \sim 1/l_\perp l_\parallel$, while the resultant electric field produced by vortex motion scales as $E \sim 1/l_\perp \tau$, leading to a *scaling ansatz* for the current in the critical regime, where $El_\perp^{1+z} = F_\pm(l_\perp l_\parallel J \Phi_0 / cT)$ and F_\pm is the universal scaling function. While F_+ and F_- are unknown, the scaling hypothesis allows current-voltage data for different temperatures to be collapsed onto F_+ above, and F_- below, T_{Bg} . The two divergent lengths cancel at $T = T_{\text{Bg}}$, giving a power-law dependence $E \sim J^{(1+z)/3}$.

Figure 2(a) shows the voltage-current curves for the irradiated crystal, taken at various temperatures for $H = 1\ \text{T}$ applied parallel to the defects. The curves clearly show a crossover from a linear to nonlinear critical regime. In Fig. 2(b) the E - J curves have been scaled according to the scaling ansatz, with an excellent collapse of the data both above and below T_{Bg} . The critical exponents ν and z , as well as the Bose glass temperature, were varied to obtain the best overall fit where deviations were kept within 20% over several decades. From this analysis we obtain $\nu = 1.67 \pm 0.10$, $z = 3.44 \pm 0.10$, and $s = \nu(z - 2) = 2.4 \pm 0.2$, where the latter is the scaling exponent for the temperature dependence of the resistivity near T_{Bg} , $\rho \sim (T - T_{\text{Bg}})^s$ in the limit of low excitation current. The values of ν and z are greater and smaller, respectively, than the values reported by Grigera *et al.*¹⁷ on twin boundaries and the values obtained from cubic (K, Ba) BiO_3 samples with columnar defects,²⁸ although the value of s is consistent with Grigera *et al.*'s result. Our value of z is also similar to that obtained from recent Monte Carlo simulations by Lidmar and Wallin²⁹ that found $z = 4.6 \pm 0.3$. Also plotted in Fig. 2(a) is the expected power-law dependence

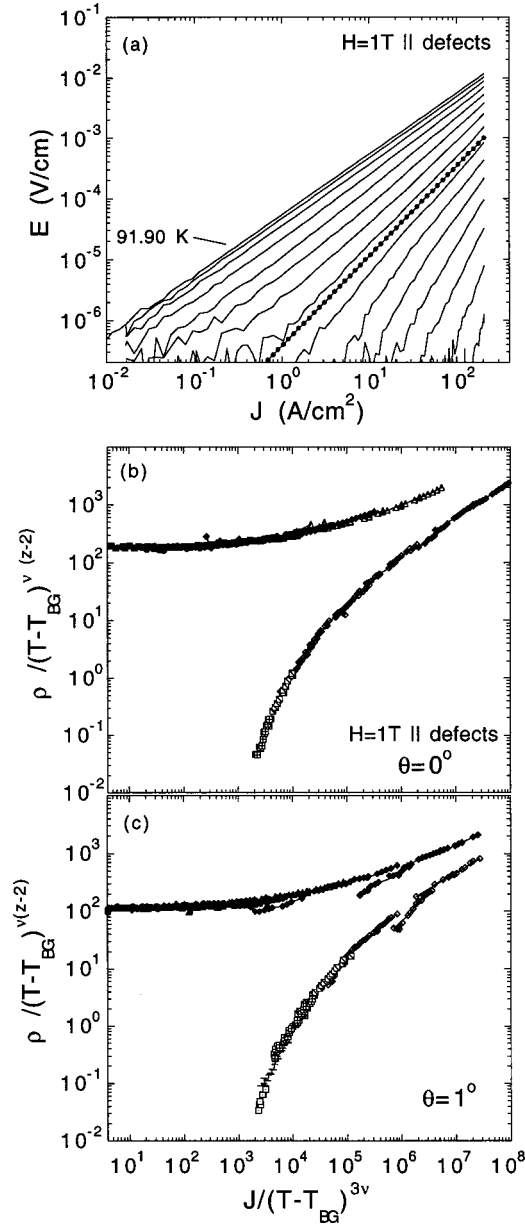


FIG. 2. (a) E - J curves of the irradiated crystal taken at $H=1$ T for $90.50 < T < 91.90$ K in intervals of 0.1 K (b) Scaling of the $H=1$ T nonlinear E - J curves ($T < 91.70$ K) with the Bose glass scaling ansatz. (c) Scaling of the $H=1$ -T voltage-current curves for $\theta=1^\circ$.

$E \sim J^{1.47}$ at T_{BG} , where we have used $z=3.44$. This power-law behavior is consistent with the experimental data, and separates the two regions of the voltage-current curves where concave upward and downward behaviors are observed. Similar analysis for $H=0.2, 0.5,$ and 2 T yielded the same critical exponents. As indicated in the inset to Fig. 1, the fractional resistivity ρ_{irr}/ρ_n at the onset of the critical regime characterized by nonohmic behavior is shifted to lower temperature with increasing field. At $H > 3$ T, the resistivity value ρ_{irr}/ρ_n falls below the resolution of our measurement and we are no longer able to perform the scaling analysis.

The values of T_{BG} obtained from scaling the current-

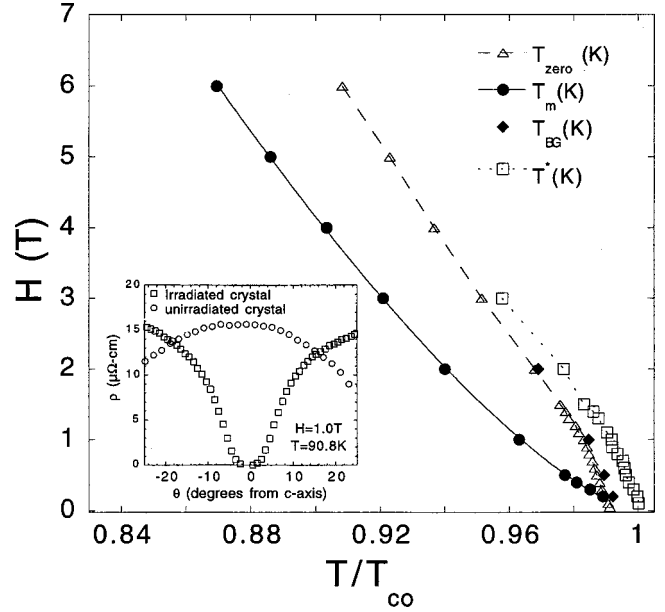


FIG. 3. Superconducting phase diagram of the 1.4-GeV $^{208}\text{Pb}^{56.4+}$ -ion irradiated and unirradiated crystals showing the first-order melting transition T_m in the reference unirradiated crystal (closed circles), zero resistivity temperature T_{zero} from a $\rho=0.01\text{-}\mu\Omega\text{ cm}$ criterion (open triangles), the Bose glass transition T_{BG} from E - J scaling (closed diamonds), and the Bose glass irreversibility line T_{irr} from the onset of nonohmic behavior after irradiation (open squares). Inset: Angular dependence of the resistivity before (open circles, $T=90.4$ K), and after (open squares, $T=90.8$ K), irradiation for $H=1$ T.

voltage curves at various magnetic fields are shown in Fig. 3 (closed diamonds), along with the first-order vortex melting line for the unirradiated reference crystal (closed circles) determined from the onset of the kink in the resistivity and the T^* line (open squares) determined from the onset of nonohmic behavior after irradiation. Also shown are the zero resistance temperatures T_{zero} (open triangles) using a $\rho=0.01\text{ }\mu\Omega\text{ cm}$ criterion, the resolution limit of our measurements with a current density of 2 A/cm^2 . At high magnetic fields above 4 T, our $\rho=0.01\text{ }\mu\Omega\text{ cm}$ criterion falls in the vortex liquid regime, and hence represents an upper bound to the Bose glass transition. At lower fields, below $H=3$ T, $\rho=0.01\text{ }\mu\Omega\text{ cm}$ resides in the nonohmic regime and closely follows the T_{BG} curve obtained from scaling. After irradiation, both T^* and T_{zero} are shifted to higher temperatures compared to the first-order melting line.

Above T_{BG} but within the critical regime, and in the limit of very low current density, the resistivity is expected to be ohmic. In this limit the function $F_+(x) \sim x$ and the resistivity should vanish as $\rho(T \rightarrow T_{BG}^+, J \rightarrow 0) \sim (T - T_{BG})^{\nu(z-2)}$.¹² In order to determine the Bose glass transition temperature above $H=3$ T, the tail of the temperature-dependent resistivity should be fitted to this power law. However, we were not able to obtain the ohmic regime since it lay below our sensitivity limit for low current excitations.

The anisotropic pinning behavior of the Bose glass is demonstrated by the plot of the angular-dependent resistivity when the magnetic field is tilted away from the columnar

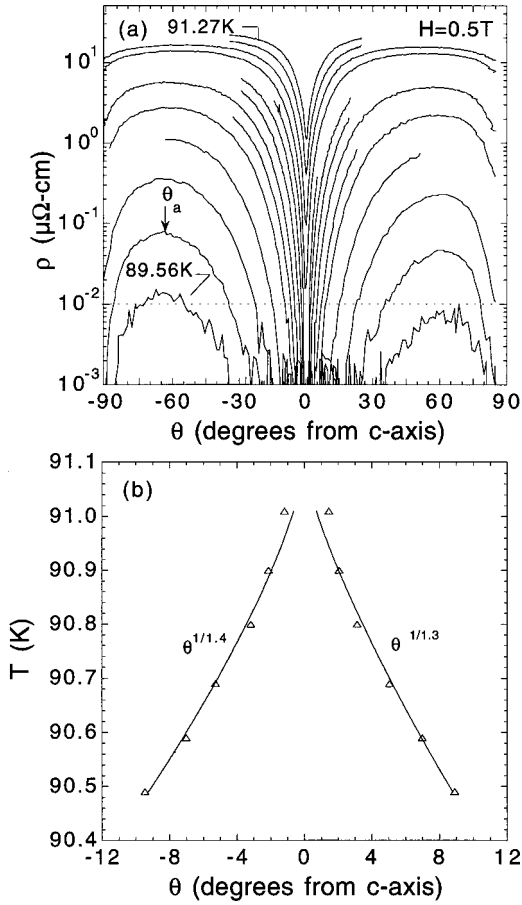


FIG. 4. (a) Angular-dependent resistivity of the irradiated crystal at $H=0.5$ T, $89.56 < T < 91.27$ K in approximate steps of 0.1 K. (b) Bose glass scaling of the angular-dependent resistivity data of (a) using $\rho=0.01$ - $\mu\Omega$ cm criterion. Other resistive criteria gave slightly higher values.

defect direction, as shown in the inset of Fig. 3. For comparison, the angular-dependent resistivity of the unirradiated crystal is also plotted. The minimum dissipation at $\theta=0^\circ$ for the irradiated sample indicates that columnar defects are most effective as pinning sites when the vortices are aligned along the defect direction. Dissipation increases with increasing angle, up to $\theta=\theta_a$, beyond which pinning by columnar defects effectively disappears and the angular dependence of the dissipation is dictated by the intrinsic superconducting anisotropy.

Within the Bose glass phase, theory predicts an infinite tilt modulus for vortices that remain aligned to the defect tracks. At some finite applied transverse field $H_\perp^c(T)$, the Bose glass state is transformed into a kinked vortex configuration.³⁰ The transition from the “lock-in” phase to the “kinked” phase is characterized by a sharp increase in the measured resistivity, due to the relatively free motion of the kinks as they move along the columnar defects. In the lock-in phase, the resistivity is effectively zero, since the vortices remain pinned along the columnar defects. As the temperature is lowered, the transverse field where the transition occurs increases. The lock-in transition is expected to scale from above as $T_{\text{Bg}}(0) - T_{\text{Bg}}(\theta) \sim |H_\perp^c|^{1/\nu}$.^{12,29} The transition cannot be

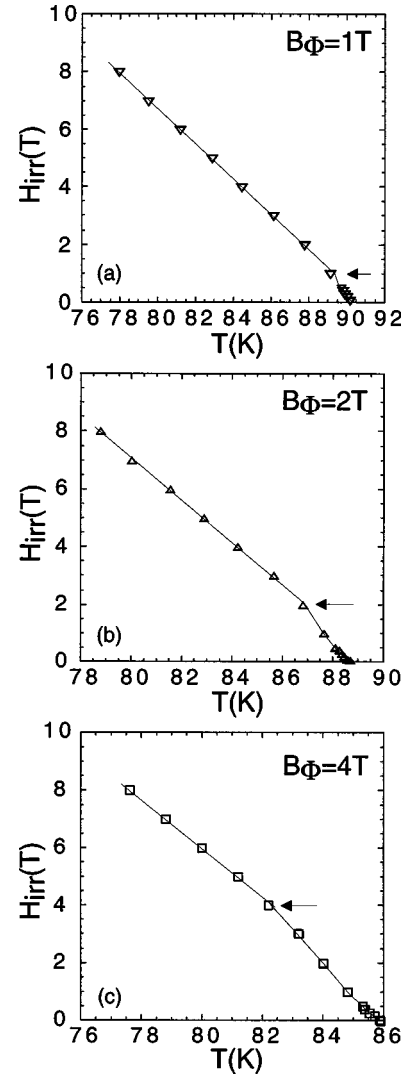


FIG. 5. Irreversibility lines of three untwinned YBCO crystals irradiated with 1.4-GeV U ions to a dose matching field of (a) $B_\phi = 1$, (b) $B_\phi = 2$, and (c) $B_\phi = 4$ T. Arrows indicate the “kink” very close to the corresponding matching field. The lines are guides for the eye.

scaled from below, since l_\parallel is essentially infinite (equal to the sample thickness) below the transition.

At $H=1.0$ T and at very small angles $-1^\circ < \theta < 1^\circ$, we measured several E - J curves at various temperatures near T_{Bg} . We can collapse the E - J data with the same scaling procedure as the $\theta=0^\circ$ data and we obtain $\nu=1.57 \pm 0.4$, $z=3.55 \pm 0.5$, and $s=\nu(z-2)=2.4 \pm 0.10$, in excellent agreement the results for $\theta=0^\circ$. This is demonstrated in Fig. 2(c), which shows scaled data for $\theta=1^\circ$. Thus within the 1° window the vortices behave as if they are perfectly aligned with the pins. Beyond 1° the data no longer can be scaled in this manner. We therefore use a different approach to investigate the lock-in transition, using the angular dependence of the resistivity.

The angular-dependent resistivity shown in Fig. 4(a) is zero within our sensitivity limit over a finite range of angles near $\theta=0^\circ$, then increases sharply with angle. We take the

intersection of the sharply rising resistivity with our sensitivity cutoff value as the operational definition of the lock-in transition. We choose a sensitivity criterion of $\rho = 0.01 \mu\Omega \text{ cm}$, the same as that used to determine T_{zero} in Fig. 3, where it gave good agreement with T_{Bg} determined from scaling the E - J curves. As shown below, other resistive criteria yield consistent results, indicating the abrupt jump in the resistance near $\theta = 0^\circ$ when the field is tilted. Therefore, we take our criterion as a reasonable estimate of the Bose glass-liquid transition at finite angle. The angular dependence of the Bose glass transition temperature using this criteria is shown in Fig. 4(b), along with best fits to the lock-in transition function $T_{\text{Bg}}(0) - T_{\text{Bg}}(\theta) \sim |H_{\perp}^c|^{1/\nu}$, where $H_{\perp}^c/H \approx \theta$ for small angles. As a check, other resistive criteria were also investigated, with consistent results for ν . From this analysis, using both $\rho = 0.05$ and $0.1 \mu\Omega \text{ cm}$ criteria, we obtained $\nu = 1.7 \pm 0.4$, in good agreement with our previous analysis. Furthermore, it is also in good agreement with recent transport and magnetization measurements along the defect direction on untwinned YBCO crystals irradiated with 4 GeV Au ions,²³ which found $\nu \approx 1.9 \pm 0.2$. However, for larger angles, the magnetization measurements diverge from the transport measurements, yielding $\nu \approx 1$. The origin of the difference between the critical exponents from magnetization and transport measurements is not yet clear. For further discussion, see Ref. 23.

Finally, we report on the kink found in the Bose glass irreversibility line of the irradiated crystal. This kink occurs very close to the matching field of $B_{\Phi} = 1 \text{ T}$ as shown in Fig. 3. Similar kinks in the irreversibility line were reported earlier in irradiated twinned YBCO crystals at $H = \frac{1}{2} B_{\Phi}$.³¹ Subsequent studies on irradiated untwinned crystals showed kinks very close to the matching field.³² A study of (K,Ba)BiO₃ with columnar defects also finds different cur-

vature in the melting line above and below the matching field, with the Bose glass transition approaching the preirradiation melting line for $H \gg B_{\Phi}$.²⁸ The kink in the irreversibility line is related to the change in pinning behavior when the density of vortices becomes greater than the defect density with increasing applied magnetic field. Figure 5 displays the T_{zero} lines for three samples cleaved from a $1500(l) \times 500(w) \times 18(t) \text{-}\mu\text{m}^3$ untwinned crystal irradiated with 1.4-GeV ²³⁸U ions to dose matching fields of $B_{\Phi} = 1, 2,$ and 4 T . Similar to the Pb-ion irradiated crystal, all three samples exhibit a kink in T_{zero} close to the matching field B_{Φ} , with a linear temperature dependence above, and positive curvature below, the kink. The linear behavior above B_{Φ} can be interpreted as a weakening of the pinning efficiency when the vortices outnumber the columnar defects.³³

In summary, we have demonstrated the Bose glass scaling behavior in a single crystal of YBCO free from twin boundary pinning. We determined the scaling exponents from voltage-current measurements near the transition temperature and found them to be in good agreement with values reported by Monte Carlo simulations. We also inferred a lock-in transition from measurements of the angular dependence of the resistivity and found the resultant critical exponent from the angular dependence to be in good agreement with the scaling analysis for $H \parallel$ defects. Finally, we demonstrated that the kink in the Bose glass irreversibility line in irradiated untwinned YBCO occurs very close to the matching field and is associated with a weakened pinning behavior when vortices outnumber the columnar defects.

This work was supported by the U.S. Department of Energy, Basic Energy Sciences—Material Sciences under Contract No. W-31-109-ENG-38 (R.J.O., W.K.K., A.M.P., and G.W.C.) and by the National Science Foundation through Grant No. DMR-0072880 (L.M.P.).

*Permanent address: Department of Physics, Western Michigan University, Kalamazoo, MI 49008.

†Permanent address: Department of Physics, University of Illinois, Chicago, IL 60607.

¹B. Khaykovich, M. Konczykowski, K. Teitelbaum, E. Zeldov, H. Shtrikman, and M. Rappaport, Phys. Rev. B **57**, R14 088 (1998).

²W. K. Kwok, R. J. Olsson, G. Karapetrov, L. M. Paulius, W. G. Moulton, D. J. Hofman, and G. W. Crabtree, Phys. Rev. Lett. **84**, 3706 (2000).

³A. M. Petrean, L. M. Paulius, W.-K. Kwok, J. A. Fendrich, and G. W. Crabtree, Phys. Rev. Lett. **84**, 5852 (2000).

⁴L. M. Paulius, W.-K. Kwok, R. J. Olsson, A. M. Petrean, V. Tobos, J. A. Fendrich, G. W. Crabtree, C. A. Burns, and S. Ferguson, Phys. Rev. B **61**, R11 910 (2000).

⁵Ruixing Liang, D. A. Bonn, and W. N. Hardy, Phys. Rev. Lett. **76**, 835 (1996).

⁶U. Welp, J. A. Fendrich, W. K. Kwok, G. W. Crabtree, and B. W. Veal, Phys. Rev. Lett. **76**, 4809 (1996).

⁷A. Schilling, R. A. Fisher, N. E. Phillips, U. Welp, W. K. Kwok, and G. W. Crabtree, Phys. Rev. Lett. **78**, 4833 (1997).

⁸F. Bouquet, C. Marcenat, E. Steep, R. Calemczuk, W. K. Kwok, U. Welp, G. W. Crabtree, R. A. Fisher, N. E. Phillips, and A. Schilling, Nature (London) **411**, 448 (2001).

⁹Y. Imry and M. Wortis, Phys. Rev. B **19**, 3580 (1979).

¹⁰M. P. A. Fisher, Phys. Rev. Lett. **62**, 1415 (1989); D. S. Fisher, M. P. A. Fisher, and D. A. Huse, Phys. Rev. B **43**, 130 (1991).

¹¹C. Reichhardt, A. v. Otterlo, and G. T. Zimányi, Phys. Rev. Lett. **84**, 1994 (2000).

¹²D. R. Nelson and V. M. Vinokur, Phys. Rev. Lett. **68**, 2398 (1992); Phys. Rev. B **48**, 13 060 (1993).

¹³R. H. Koch, V. Foglietti, W. J. Gallagher, G. Koren, A. Gupta, and M. P. A. Fisher, Phys. Rev. Lett. **63**, 1511 (1989).

¹⁴P. L. Gammel, L. F. Schneemeyer, and D. J. Bishop, Phys. Rev. Lett. **66**, 953 (1991).

¹⁵W. Jiang, N.-C. Yeh, D. S. Reed, U. Kriplani, D. A. Beam, M. Konczykowski, T. A. Tombrello, and F. Holtzberg, Phys. Rev. Lett. **72**, 550 (1994).

¹⁶D. S. Reed, N.-C. Yeh, M. Konczykowski, A. V. Samoilov, and F. Holtzberg, Phys. Rev. B **51**, 16 448 (1995).

¹⁷S. A. Grigera, E. Morré, E. Osquiguil, C. Balseiro, G. Nieva, and F. de la Cruz, Phys. Rev. Lett. **81**, 2348 (1998).

¹⁸V. K. Vlasko-Vlasov, L. A. Dorosinskii, A. A. Polyanskii, V. I. Nikitenko, U. Welp, B. W. Veal, and G. W. Crabtree, Phys. Rev. Lett. **72**, 3246 (1994).

¹⁹M. Oussena, P. A. J. de Groot, S. J. Porter, R. Gagnon, and L. Taillefer, Phys. Rev. B **51**, 1389 (1995).

- ²⁰W. K. Kwok, J. A. Fendrich, V. M. Vinokur, A. E. Koshelev, and G. W. Crabtree, *Phys. Rev. Lett.* **76**, 4596 (1996).
- ²¹W. K. Kwok, J. A. Fendrich, C. J. van der Beek, and G. W. Crabtree, *Phys. Rev. Lett.* **73**, 2614 (1994).
- ²²A. Mazilu, H. Safar, M. P. Maley, J. Y. Coulter, L. N. Bulaevskii, and S. Foltyn, *Phys. Rev. B* **58**, R8909 (1998).
- ²³A. W. Smith, H. M. Jaeger, T. F. Rosenbaum, A. M. Petrean, W. K. Kwok, and G. W. Crabtree, *Phys. Rev. Lett.* **84**, 4974 (2000).
- ²⁴L. Civale, A. D. Marwick, T. K. Worthington, M. A. Kirk, J. R. Thompson, L. Krusin-Elbaum, Y. Sun, J. R. Clem, and F. Holtzberg, *Phys. Rev. Lett.* **67**, 648 (1991).
- ²⁵J. F. Ziegler, J. P. Biersack, and U. Littlemark, *The Stopping Range of Ions in Solids* (Pergamon, New York, 1986), p. 70.
- ²⁶J. P. Biersack and L. G. Haggmark, *Nucl. Instrum. Methods* **174**, 257 (1980).
- ²⁷J. A. Fendrich, U. Welp, W. K. Kwok, A. E. Koshelev, G. W. Crabtree, and B. W. Veal, *Phys. Rev. Lett.* **77**, 2073 (1996).
- ²⁸T. Klein, A. Conde-Gallardo, I. Joumard, J. Marcus, C. J. van der Beek, and M. Konczykowski, *Phys. Rev. B* **61**, R3830 (2000).
- ²⁹J. Lidmar and M. Wallin, *Europhys. Lett.* **47**, 494 (1999).
- ³⁰T. Hwa, D. R. Nelson, and V. M. Vinokur, *Phys. Rev. B* **48**, 1167 (1993).
- ³¹L. Krusin-Elbaum, L. Civale, G. Blatter, A. D. Marwick, F. Holtzberg, and C. Feild, *Phys. Rev. Lett.* **72**, 1914 (1994).
- ³²A. W. Smith, H. M. Jaeger, T. F. Rosenbaum, W. K. Kwok, and G. W. Crabtree, *Phys. Rev. B* **59**, R11 665 (1999).
- ³³L. Radzihovsky, *Phys. Rev. Lett.* **74**, 4923 (1995).